Electronic Supporting Information

Dual-signalled magneto-optical barcodes with lanthanide-based molecular cluster-aggregates

Diogo Alves Gálico,[a] and Muralee Murugesu[a]*

[a] Department of Chemistry and Biomolecular Sciences, University of Ottawa, Ottawa, Ontario

K1N 6N5, Canada.

Email: m.murugesu@uottawa.ca

Experimental Section

Synthesis of {[Ln$_6$(teaH)$_6$(NO$_3$)$_6$]: The synthetic procedure follows the previously reported synthesis.[S1] Ho(NO$_3$)$_3$·6H$_2$O (0.6 mmol) was dissolved in MeOH/CH$_2$Cl$_2$ (5 mL : 15 mL), followed by the addition of triethanolamine (1.2 mmol) and triethylamine (4.8 mmol). After a few minutes, the reaction mixture resulted in a clear pink solution. This solution was stirred for four hours. During this time, a small amount of precipitate formed. The solution was filtered and layered with Et$_2$O. After two days, yellow crystals of [Ho$_6$(teaH)$_6$(NO$_3$)$_6$] appeared in an approximate yield of 58 % (crystalline product).

For {Er$_6$}, the same procedure was followed using 0.6 mmol of Er(NO$_3$)$_3$·6H$_2$O. Yield = 62 % (pink crystalline product).

For {Ho$_3$Er$_3$}, the same procedure was followed using 0.3 mmol of Ho(NO$_3$)$_3$·6H$_2$O and 0.3 mmol of Er(NO$_3$)$_3$·6H$_2$O. Yield = 56 % (orange crystalline product).

Characterisation:

FTIR spectra were obtained in a Nicolet 6700 FT-IR Spectrometer (Thermo Scientific).

PXRD diffractograms were obtained in a Rigaku Ultima IV Diffractometer using Cu Kα filtered radiation (λ = 1.5401 Å).

ICP analysis was performed in a 5110 ICP-OES Instrument (Agilent).

MCD measurements were performed on a Jasco J-1700 CD spectrometer and an Oxford SpectromagPT cryogen-free magneto-optical superconducting magnet system as depicted in Scheme S1. All the spectra were obtained in the 300 – 850 nm range, with three accumulations, a bandwidth of 2 nm, and a scan speed of 1000 nm/min. The samples were prepared as a 0.1 mg mL^{-1} aqueous solution.
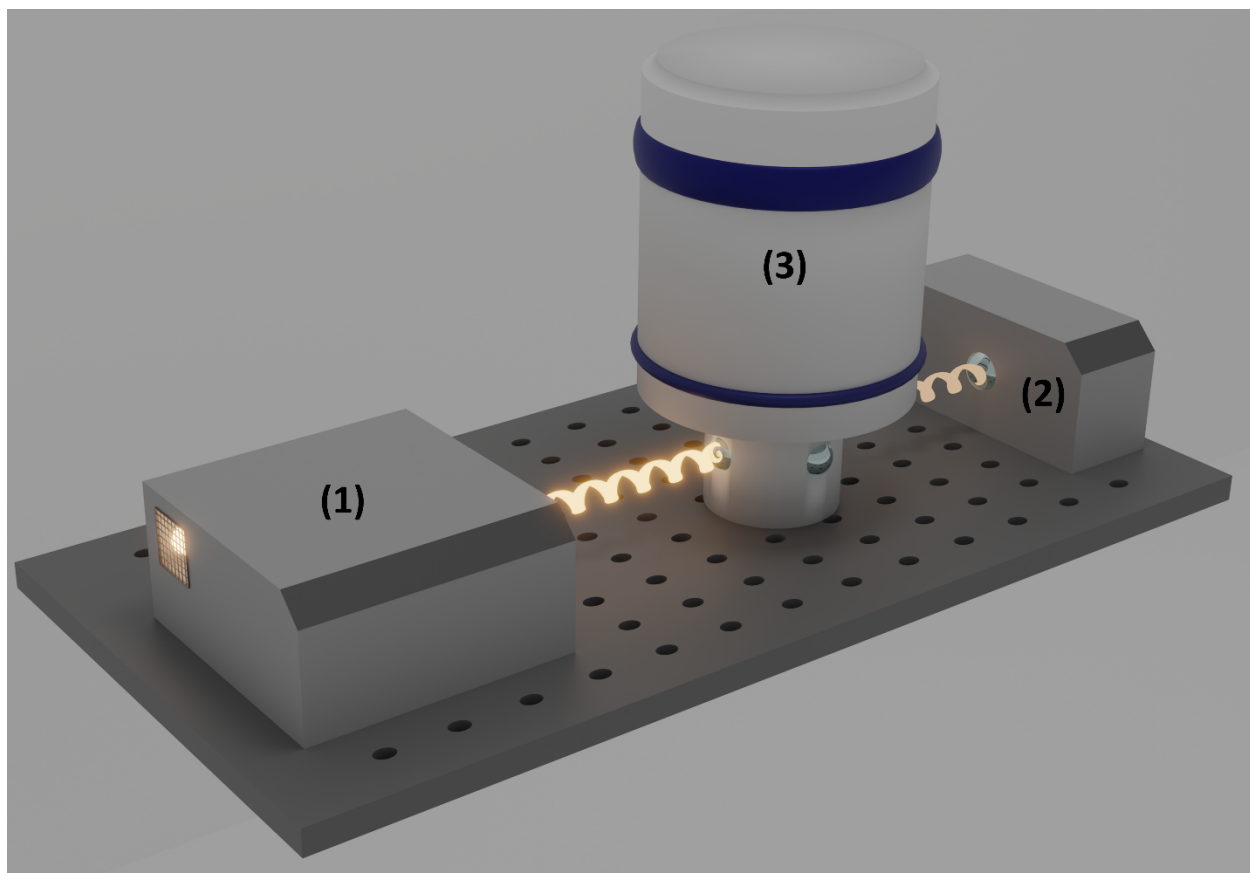
Scheme S1: Schematic representation of the experimental setup. The unpolarized light from a Xe lamp is circularly polarized inside the Jasco J-1700 CD spectrometer **(1)** monochromator and reaches the **(2)** detector after interacting with the sample. The sample is placed in a 1 cm optical path quartz cuvette and placed inside the **(3)** Oxford SpectromagPT cryogen-free magneto-optical superconducting magnet system.

Figures and Tables
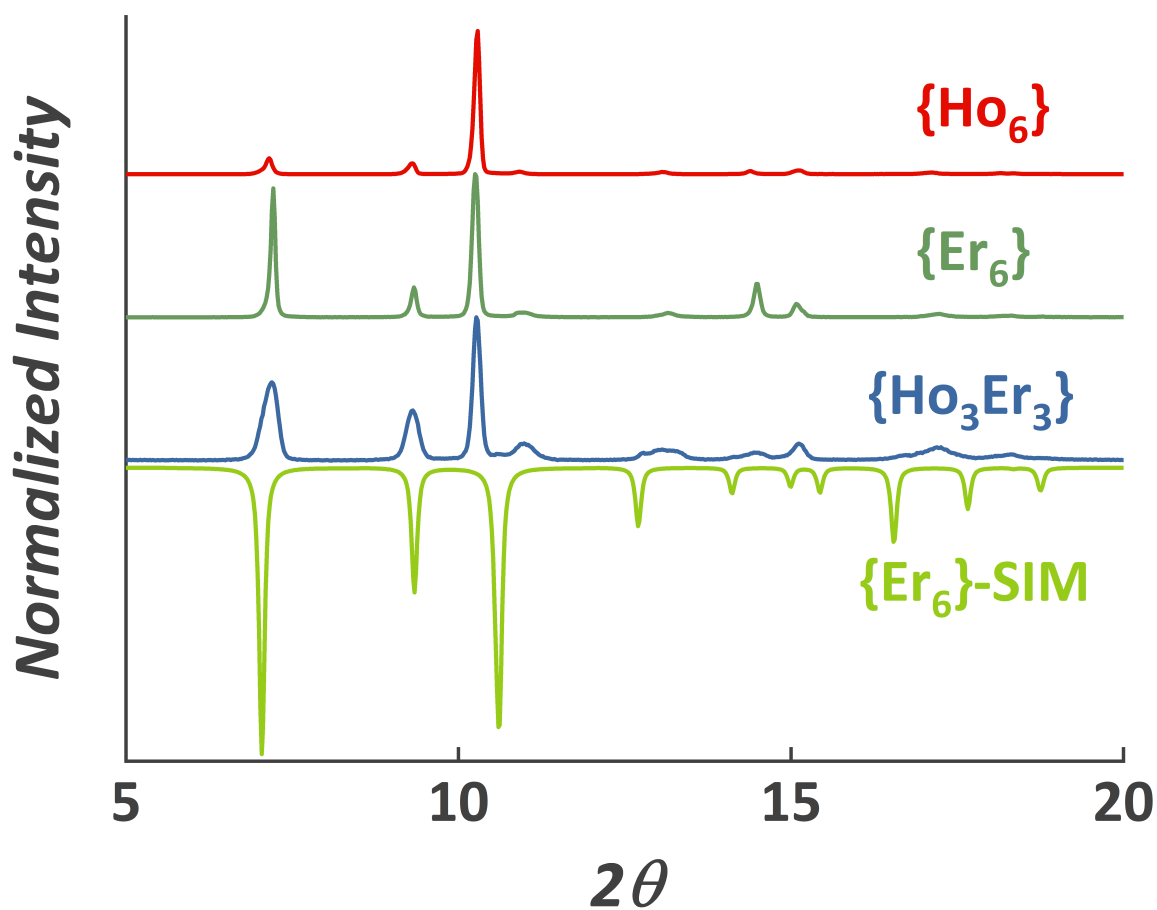
Figure S1: Experimental PXRD diffractograms for **{Ho$_6$}**, **{Er$_6$}**, and **{Ho$_3$Er$_3$}** MCAs compared with the simulated for **{Er$_6$}** (CCDC number: 1876163).
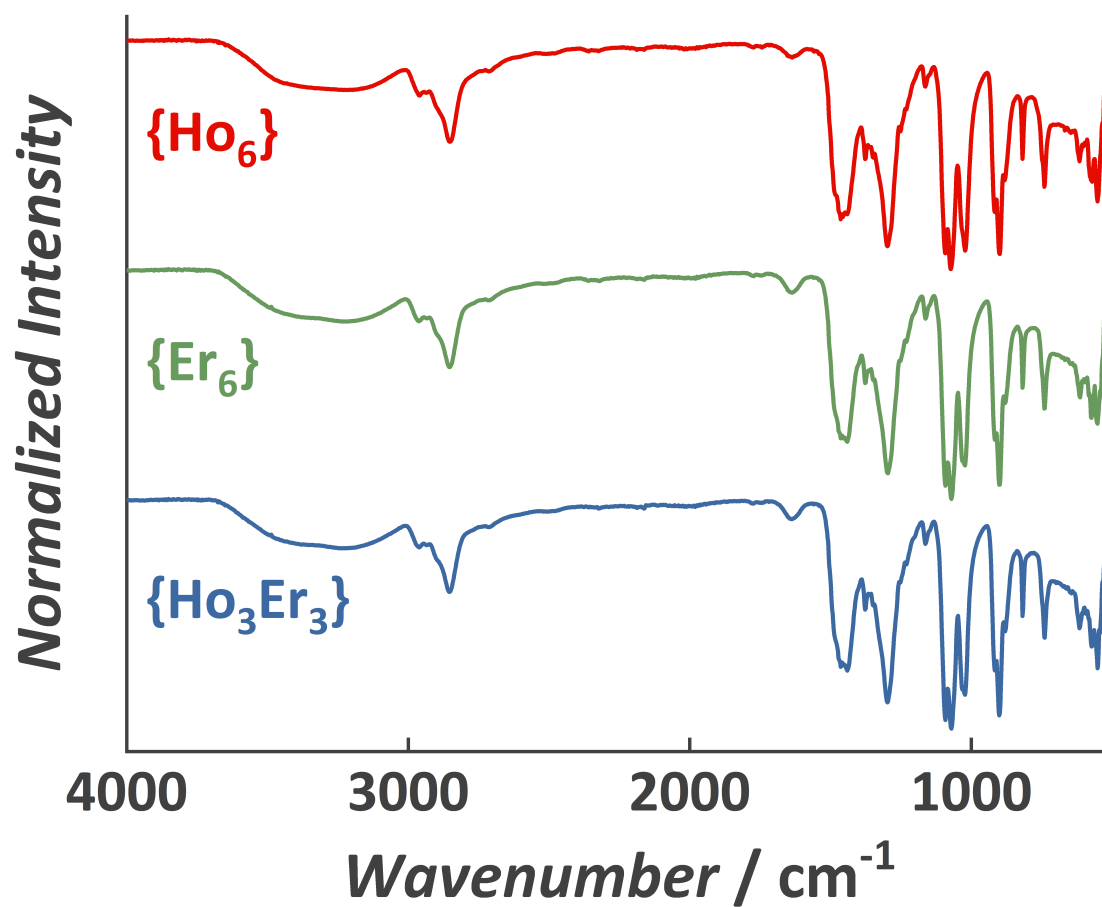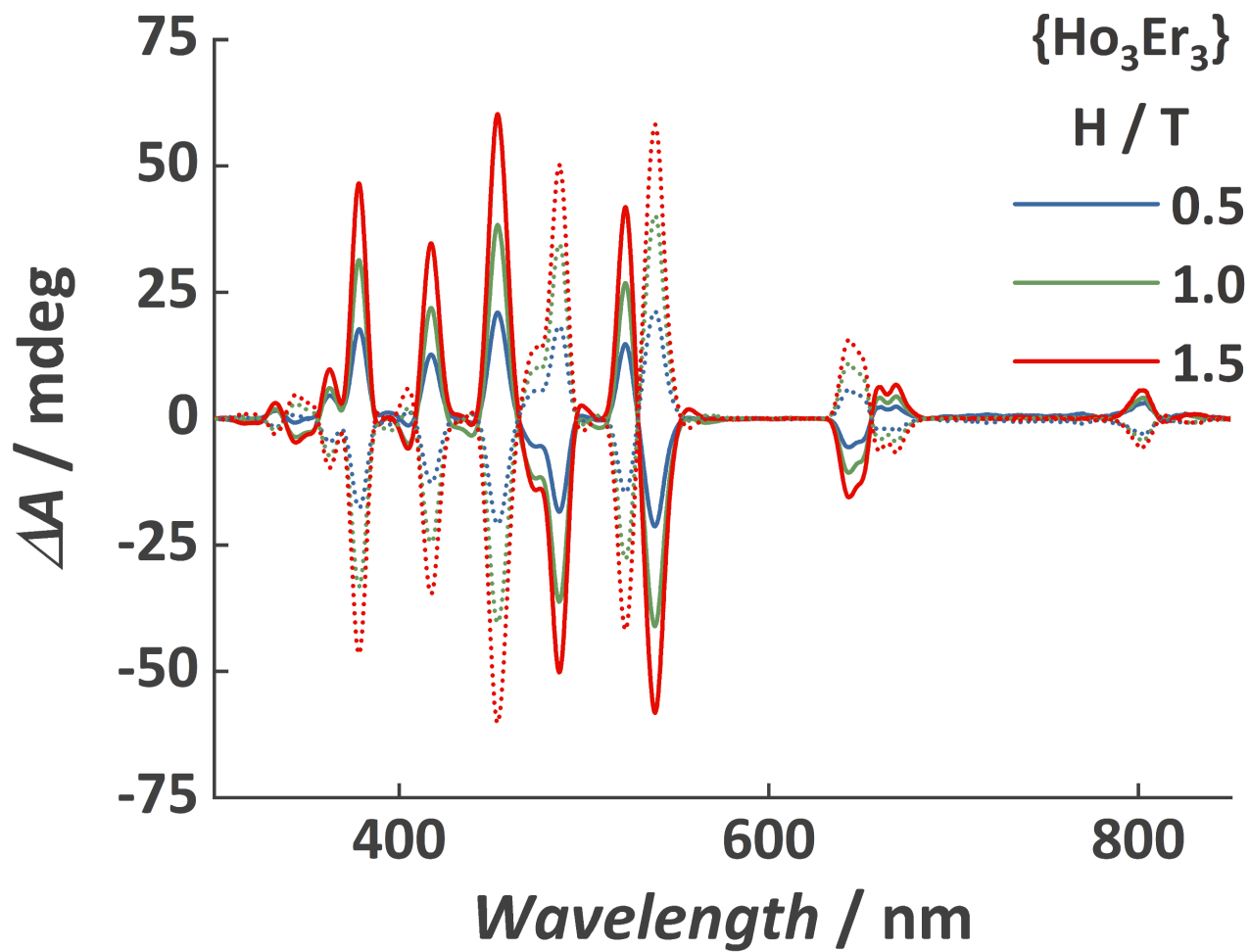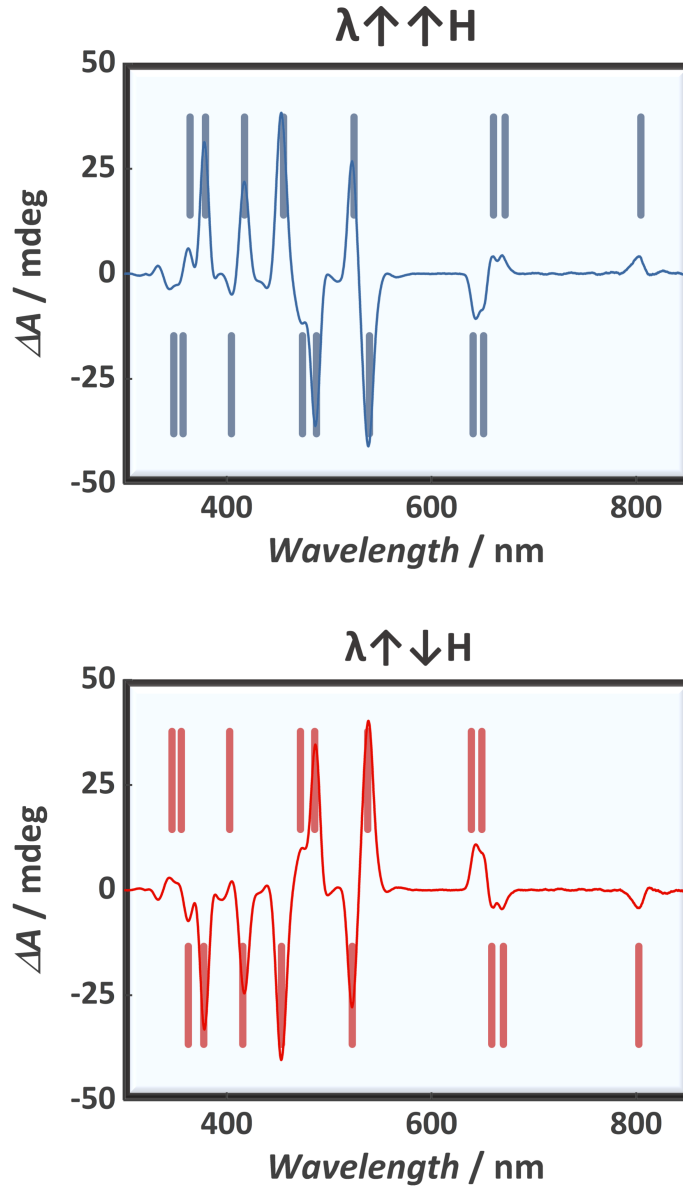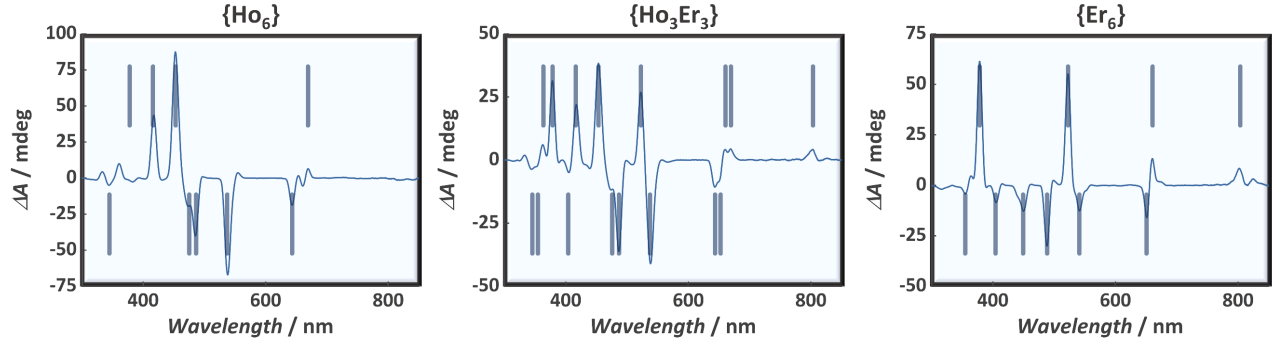
Figure S2: FTIR spectra for {Ho₆}, {Er₆}, and {Ho₃Er₃} MCAs.

Figure S3: MCD spectra for **{Ho₃Er₃}** MCA obtained at 25 °C and under different applied magnetic fields. Dotted spectra refer to H = -0.5, -1.0, and -1.5 T magnetic fields.

Figure S4: Overlay between the MCD spectrum and the magneto-optical barcode read-out for **{Ho₃Er₃}** MCA with an applied magnetic field of (top) 1.0 T and (bottom) -1.0 T. This figure demonstrates the extra security feature attained in magneto-optical barcodes; the mirror-image obtained when reversing the magnetic field.

Figure S5: Comparison between the magneto-optical barcode read-out for **{Ho₆}**, **{Er₆}**, and **{Ho₃Er₃}** MCAs with an applied magnetic field of 1.0 T. This figure evidence the highest spectral complexity for the heterometallic MCA magneto-optical barcode.

Table S1: Energy levels of Ho^{III} and Er^{III}. Energies obtained from Carnall.[S2]

Ho^{III}		Er^{III}	
Wavenumber / cm^{-1}	Assignment	Wavenumber / cm^{-1}	Assignment
30799	$^5G_2 \leftarrow {}^5I_8$	33319	$^2P_{1/2} \leftarrow {}^4I_{15/2}$
29947	$(^3F_4, {}^3K_6) \leftarrow {}^5I_8$	28224	$(^2K_{15/2}, {}^4G_{7/2}) \leftarrow {}^4I_{15/2}$
28875	$(^5G_3, {}^3L_9) \leftarrow {}^5I_8$	27637	$^4G_{9/2} \leftarrow {}^4I_{15/2}$
27678	$(^5G_5, {}^3H_6) \leftarrow {}^5I_8$	26631	$^4G_{11/2} \leftarrow {}^4I_{15/2}$
26058	$^3K_7 \leftarrow {}^5I_8$	24756	$^2H_{9/2} \leftarrow {}^4I_{15/2}$
25859	$^5G_4 \leftarrow {}^5I_8$	22712	$^4F_{3/2} \leftarrow {}^4I_{15/2}$
23987	$^5G_5 \leftarrow {}^5I_8$	22376	$^4F_{5/2} \leftarrow {}^4I_{15/2}$
22179	$^5G_6 \leftarrow {}^5I_8$	20715	$^4F_{7/2} \leftarrow {}^4I_{15/2}$
21267	$^3K_8 \leftarrow {}^5I_8$	19337	$(^2H_{11/2}, {}^4S_{3/2}) \leftarrow {}^4I_{15/2}$
21039	$^5F_2 \leftarrow {}^5I_8$	15455	$^4F_{9/2} \leftarrow {}^4I_{15/2}$
20594	$^5F_3 \leftarrow {}^5I_8$	12597	$^4I_{9/2} \leftarrow {}^4I_{15/2}$
18538	$^5F_4 \leftarrow {}^5I_8$	-	-
18381	$^5S_2 \leftarrow {}^5I_8$	-	-
15456	$^5F_5 \leftarrow {}^5I_8$	-	-
13212	$^5I_4 \leftarrow {}^5I_8$	-	-

References

[1] D. A. Gálico, J. S. Ovens and M. Murugesu, *Nanoscale*, 2020, **12**, 11435—11439.

[2] W. T. Carnall, H. Crosswhite and H. M. Crosswhite, *Energy level structure and transition probabilities in the spectra of the trivalent lanthanides in LaF₃*, Argonne Nat. Lab. 78-XX-95 Rep., 1977